Invest to Save Budget

Improved Air Quality Forecasting
Invest to Save Report ISB52-06

Boundary Layer Measurements of Dispersion Model Parameters using Dual Doppler Lidar at Malvern, UK

By

F Davies, C Collier, A Holt, D Middleton, G Pearson, S Siemen, DV Willetts & RI Young.

3 July 2003

© Copyright 2003

Authorisation

Prepared by	Dr RI Young
Title	
Signature	
Date	July 2003
Location	QinetiQ Malvern

Principal authors	Dr GN Pearson
Appointment	QinetiQ Fellow, Remote Sensing
Location	QinetiQ
Principal authors	Professor DV Willetts
Appointment	QinetiQ Senior Fellow, Remote Sensing
	QinetiQ
Principal authors	Dr D Middleton
Appointment	Air Quality Scientist
Location	Met Ofice, London
Principal authors	Dr F Davies
Appointment	Research Fellow, ISB-52
Location	Salford University
Principal authors	Professor C Collier
Appointment	Dean, Faculty of Science, Engineering and Environment
Location	Salford University
Principal authors	Professor A Holt
Appointment	Propagation and Remote Sensing Research group.
Location	Essex University
Principal authors	Dr S Siemen
Appointment	Research Fellow, ISB-52
Location	Essex University
Principal authors	Dr RI Young
Appointment	Project Manger, Remote Sensing
Location	QinetiQ

Record of changes

Issue	Date	Detail of Changes
1.0	3 July 2003	First Release

EXECUTIVE SUMMARY

This report ISB52-06 was produced under Project 52 of the Invest to Save Budget, or ISB. The aim of this project is to improve atmospheric pollution dispersion models with the goal of improving air quality forecasting. During the project life, the team will be developing a better understanding of airflow near the earth's surface, focussing especially on urban meteorology. This will be achieved through the gathering of accurate 3-Dimensional wind flow data using laser radars, also called lidars, and by incorporating that new knowledge into the dispersion models.

A lidar is similar to conventional radar but uses an invisible, eye-safe, laser beam as its source of radiation. The great advantage of lidars for monitoring wind flow is that they can make more precise measurements than conventional radars and can probe to greater heights than most tall masts. In addition, lidars can make measurements in regions of the lower atmosphere above a city, which would be inaccessible to either aircraft or tethered balloons.

The lidars work by measuring the Doppler shift of light back-scattered from fine aerosol particles (water droplets, dust, etc) suspended within the atmosphere. The line of sight velocity component of the wind is then calculated. By sampling at different angles, and combining results from the two lidars, a picture of the three dimensional airflow in a scanned region can be assembled. Typically the scanned volume will be a few cubic km with the probes separated by up to 10 km.

This report summarises the results from the first field trial with two such Doppler Lidars being worked in symbiosis. The work described here includes the deployment and alignment of the two lidars near Malvern, UK, the comparison of the two lidars when pointing in similar directions and sampling a common flow, and the results when the lidar beams were aligned to intersect. So far as the authors could establish, these trials represent the first time that two lidars have been set up to allow the recording of Doppler velocities from an intersection region, and thus reduce the number of unknowns when solving for the flow.

Dual Doppler Lidar is a new technique developed for this project in order to exploit new laser technology to obtain atmospheric measurements that a single instrument cannot make. A single lidar returns the Doppler velocity along the line of site of the laser pulses. A dual lidar allows velocity components to be estimated by solving for the flow where the beams intersect. This necessitates careful siting and alignment of the two lidars. In addition, the data also facilitates the estimation of a number of important parameters that are used or calculated in atmospheric dispersion models.

In this trial, we have used the Doppler Lidar data to investigate variables from the UK Met Office NAME model, and the ADMS model. Both models are much used in the United Kingdom. The NAME model is used for air quality forecasting, source apportionment, accident and emergency simulations, episode analysis, and long range transport of pollutants and volcanic ash. The ADMS model is used in statutory local air quality management by local authorities involved in air quality reviews and assessments under the Environment Act 1995. This can include mapping of current air quality, and forecasts of projected air quality for several years ahead, based upon various planning or traffic management scenarios. ADMS is also used for environmental impact assessment and applications to the Environment Agency for large developments, such as power stations and industrial sources. Other dispersion models are also used in such work, but time precludes their study here.

This report summarises the results from the first trial, and compares the values calculated by these dispersion models used in air quality forecasting. It outlines the methods used to derive quantities from lidar data. The report ends by considering the lessons learned in readiness for the next, urban, field trial.

List of contents

Authorisation		**i**
Record of changes		**ii**
Executive Summary		**iii**
List of contents		**iv**
1	**Introduction**	**1**
2	**Equipment description**	**1**
3	**Site / data configuration**	**2**
4	**Weather Summary**	**4**
5	**Summary of retrieved data and derived parameters**	**6**
6	**Results**	**8**
7	**Boundary Layer Depth**	**16**
8	**Visualisation**	**29**
9	**Summary**	**31**
10	**References**	**32**
11	**Glossary**	**33**
A1	**Appendix**	**34**
12	**Acknowledgements**	**36**
13	**Disclaimers**	**36**
14	**Distribution list**	**36**

1. INTRODUCTION

A field trial involving simultaneous measurement of wind velocity and turbulence by two 10 μm Doppler lidar systems has been conducted in March 2003. The two lidar systems have been developed and built by QinetiQ, Malvern. The development of the first lidar system (the Salford University lidar) was conducted under a previous contract, but the development of an identical second lidar system (the QinetiQ lidar) was conducted under the first phase of this project. This was therefore the first time that two identical lidar systems have been used to make simultaneous measurements of the wind field. The use of two lidar systems enabled the independent measurement of two components of the wind flow simultaneously on a second by second basis.

The trial was conducted near to the QinetiQ site in Malvern, Worcestershire. The location of the trial enabled the smooth running of the deployment of the systems throughout the trial due to the technical support available from the nearby site. This was deemed necessary since it was the first time that these state-of-the-art research instruments had been used for the continuous measurements over any length of time. The added benefit of staying in Malvern was the local knowledge and availability of good sites for the deployment of the systems. The two lidar sites used were approximately 3 km apart which was ideal in enabling the two lidar beams to cross at an angle approaching the 90° required to make separate measurements of the two components of the horizontal wind field.

The key observations of the March trial where made from the 17th to the 19th March 2003. The weather during the three days of the trial was dominated by the high pressure system which was situated over the UK. The mornings started of very cold and misty, with the mist clearing during the day. The visibility was poor but the afternoons were mostly sunny with little cloud cover. At the start of the trial the wind was primarily from the east but on the last day of the trial it was almost calm and the wind direction was very changeable.

2. EQUIPMENT DESCRIPTION

The two lidar systems have identical key features. Their operating wavelength is 10.6 μm with a range resolution of 112 m. Other system characteristics are detailed in table 1 of report ISB52-04. The minimum ranges of the systems are determined by the back reflections of the individual optical components within the lidar. The maximum ranges are dependent upon the alignment of components within the system and the aerosol loading of the atmosphere. The two lidar systems consequently show slightly different minimum and maximum ranges, due to their different alignments. These maxima and minima vary under different atmospheric conditions. The minimum and maximum ranges are approximately 700 m and 9000 m.

The basic set-up of the two systems was detailed in report ISB52-02. The design involves a TEA (Tranverse Excitation Atmospheric) laser along with two CW (continuous wave) lasers. One CW laser and the TEA laser are used to provide the atmospheric pulsed laser signal whilst the other CW laser is used as a reference signal for the heterodyne detection of the returning atmospheric signal. The pulse repetition frequency (PRF) of the two systems can be increased but the data acquisition rate is limited by the ability of the computer to keep up with signal processing.

The signal processing procedure is detailed in Pearson and Collier (1999) and uses a scheme based on correlogram accumulation with a discrete spectral peak estimator (Rye and Hardesty, 1993). Accumulation of the return signal is carried out to improve the estimate of the calculated Doppler velocity. The amount of accumulation can be varied and this along with the PRF are inputs to the system processing procedure. The processing is done in real time enabling the continuous monitoring of the system performance.

3. SITE / DATA CONFIGURATION

The field trial was conducted in the vicinity of the QinetiQ base at Malvern, Worcestershire. The QinetiQ lidar was based permanently at the QinetiQ site. On the 17th March, the first day of the trial, the Salford lidar was also sited at the QinetiQ site, approximately 25 m from the QinetiQ lidar. On the 18th and 19th March the Salford lidar was moved to the Three Counties Show ground, which was approximately 3 km south of the QinetiQ site. The longitude and latitude of these sites is detailed in table 1.1 of report ISB52-05. The two sites (QinetiQ site and Three Counties show ground) were both approximately 1.5 km east of the ridge of the Malvern hills. The other details of the site are discussed in section 2 of ISB52-5. A summary of the data sets from two lidars are detailed in table 3.1 and 3.2 of ISB52-05.

The co-location of the two lidars at the QinetiQ site, on the 17th Match 2003, enabled a direct comparison of the data from the two lidar systems. This was an important exercise to validate the set-up and data retrieval of the two systems.

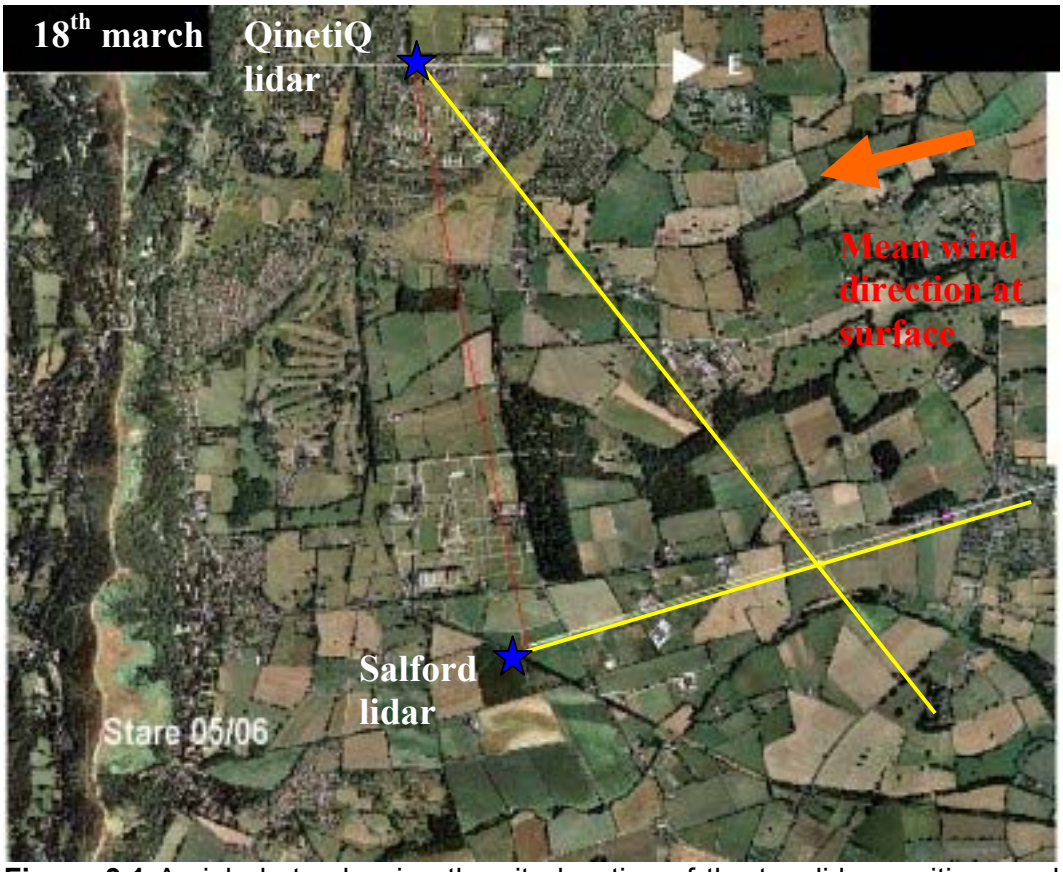

Figure 3.1 Aerial photo showing the site location of the two lidar positions and the line of sight stare angles for data set serial 04-06 (yellow lines). The green diamond

denotes the intersection point of the two beams. The mean wind direction for this data set is shown to be east-north-easterly.

Dual Doppler lidar data was collected on the 18th and 19th March using three different line-of-sight configurations. These are detailed in table 3.3 of report ISB52-05. Figure 3.1 shows the configuration for the data sets serial 04-06 which were taken from 17:58 - 18:50 pm on the 18th March 2003.

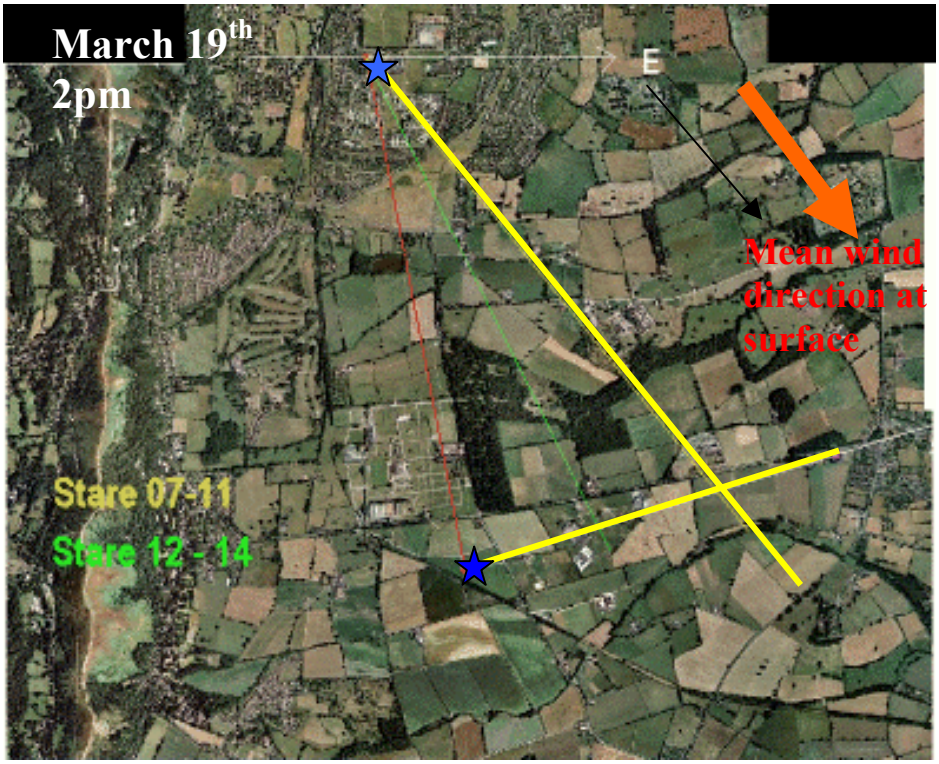

Figure 3.2 As for figure 3.1 but for data sets serial 07-11.

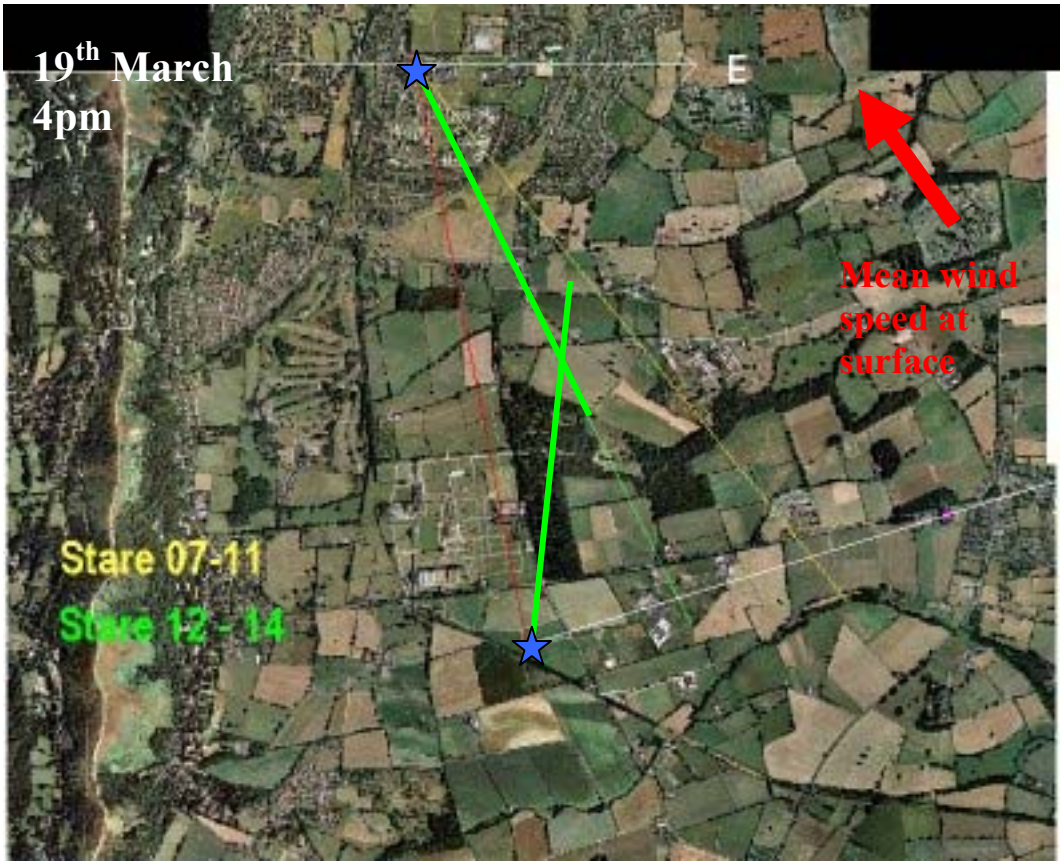

Figure 3.3 As for figure 3.1 but for data sets serial 12-13.

Figures 3.2 and 3.3 show the line of sight configurations and crossing points for the data sets 07-11 and 12-13 respectively. Both these sets of data were taken on the 19th March 2003. The wind direction calculated from a VAD scan at 1:30 pm showed the mean wind direction to be north-north-westerly, as shown in figure 3.2. By 4:00 pm the wind direction was south-south-easterly, as shown in figure 3.3. The mean wind speed on 19th March was only about 1 m s^{-1}.

4. WEATHER SUMMARY

The weather was summarised as Analysis charts for 18 &19 March 2003 which appeared in an earlier ISB52 report, MS6 part 1, Figures 2.1 & 2.2.

Before the trial, on Tuesday 11 March 2003, high pressure was to the West of the British Isles; showery rain had passed the British Isles on the 12th; then high pressure was centred over Scotland on Thursday 13 March 2003 (first day of measuring) and the UK was mainly dry with broken cloud; the centre of the high was over the North Sea on Friday 14 March 2003 and the UK had a pleasant sunny day. On Saturday 15 and Sunday 16 March 2003 it was also largely dry & sunny; from Monday 17 to Wednesday 19 March 2003 to country was still under anti-cyclonic conditions, warm and dry, with fog or some frosts at night. On Thursday 20 March 2003 there was a front over the Irish Sea up to S. Scotland. During the trial, excepting on the Sunday (when data were not taken) the weather was anti-cyclonic, and cloud cover slight and winds speed light and variable (as can be seen from the plots of input and output data for ADMS later in this report (Section 7). These plots show that according to ADMS, a deep (for the time of year, March) diurnal boundary layer developed each day, consistent with largely clear skies and dry sunny weather each day.

Date & Time (UTC)	Weather	Location
17 March 2003 16:30	13 C. 5-6 m s^{-1} from NE Hazy	Co-located at QinetiQ site. VADs performed comparing system performance & alignment.
18 March 2003 16:40	9.5 C. 3-4 m s^{-1} from E Visibility poor	QinetiQ lidar at QinetiQ site. Salford lidar at Three Counties Shows Site.
19 March 2003 14:00	14 C. 0.5-1.5 m s^{-1} Variable direction Hazy	QinetiQ lidar at QinetiQ site. Salford lidar at Three Counties Shows Site.

Table 3.1 Summary of weather for the key Malvern Trial dates 17-19 March 2003

5. SUMMARY OF RETRIEVED DATA AND DERIVED PARAMETERS

Report ISB52-03 section 2 identified the key parameters and consequently the required scan patterns needed for validation of the dispersion models. The conclusion was that the measurement of the height of the top of the planetary boundary was of top priority. Profiles of wind speed, wind direction and turbulence were also required. To achieve a set of observations representative of the statistics of pollution dispersal phenomena it was also recommended to dwell along one line of site for at least 10 minutes.

Three basic types of scan techniques can be used;

- VAD (or Azimuth) scan (which sweeps out an inverted cone at fixed elevation angle),
- RHI (or Elevation) scan (which sweeps a vertical semicircle or sector of a circle for a fixed azimuth),
- Fixed Beam (Stare) (which maintains a fixed elevation and fixed azimuth for a specified sampling period, say 10-15 minutes, long enough for reliable turbulence statistics).

A combined technique has been developed for this study:

- Dual Fixed Beam: Data from two Fixed Beams combined at their intersection point.

The lidar systems both have the capability of scanning the laser beam in azimuth and elevation. The QinetiQ system is a commercial system and can scan 0º - 360º in azimuth and 0º to 180º in elevation. The Salford University scanner was built in house and is limited to scan 0º - 295º in azimuth and 0º to 42º in elevation. Table 5.1 outlines the scanning techniques and the meteorological parameters obtained from the scan and the required length of the scan.

Scan Technique	Measured Parameter	Derived Parameter	Required length of scan (minutes)*
Fixed Beam	Radial wind velocity profile, v_r Radial wind velocity variance profile, v'^2_r System estimation error	Energy dissipation rate , ε Integral length scale, L_i Integral time scale, T	15
Vertically pointing fixed beam	Vertical velocity profile, w Vertically velocity variance profile, w'^2	Temperature flux, w't' Sensible heat flux at the surface, H Convective velocity scaling , w*	15
Dual Fixed beam⊗	Profiles of the two components of horizontal wind, u and v Profile of variances, u'^2 and v'^2	Energy dissipation rate , ε Integral length scale, L_i Integral time scale, T	15

*time includes time needed for taking of noise files for data processing procedure

⊗ wind direction profile needed to transpose radial winds to u and v components

VAD (azimuth scan)	Wind speed profile, u Wind direction profile Back-scatter Intensity profile System offset	Boundary layer height	15
RHI (elevation scan)	Profiles of area averaged values for u, v and w Profiles of area averaged values for u'w' and v'w'	Friction velocity, u* Roughness length scale, z_0 Roughness displacement height, d (N.B. for these parameters measurements must be within the surface layer)	30

Table 5.1 Parameters measured and derived from the various scan strategies

Using the fixed lidar beam values for the kinetic energy dissipation rate, integral length scale can be derived from the power spectra (Gal-Chen *et al* 1992, Davies *et al* 2003). The integral timescale can be estimated from the velocity lag autocorrelation curve (Drobinski *et al* 2000).

From using a vertically pointing fixed beam the convective velocity scaling can be estimated (Mayor *et al* 1997). From this an estimate of the heat flux, w't' and sensible heat flux at the surface, H, can then be calculated (Gal-Chen et al 1992).

6. RESULTS

The full complement of data that is available from this field trial is extensive and only a sample it discussed in this report. The results for data set serial 05 is shown here as an example of the trial data output.

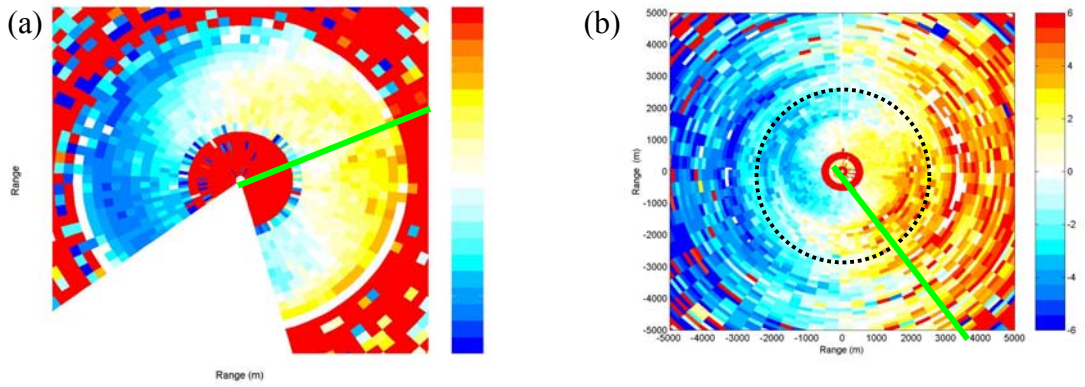

Figure 6.1 VAD scans from (a) the Salford lidar, (x and y co-ordinates on the graph are both -2000 to 2000 m) and (b) the QinetiQ lidar, (x and y co-ordinates on the graph are -5000 to 5000 m). The dotted line shows the approximate coverage of the Salford lidar. The velocity colour bar is from -6 to 6 ms^{-1}. The two lines show the stare angles shown in figure 3.1.

Initially VADs were conducted with both lidar system. These are shown in figure 6.1. The VADs show the mean wind direction and wind speed at each level through the atmosphere at approximately 16:30 on the 18th March 2003. Figure 6.1 also shows the stare angles serial 05 (see table 3.3 of report ISB52-05) as shown in figure 3.1.

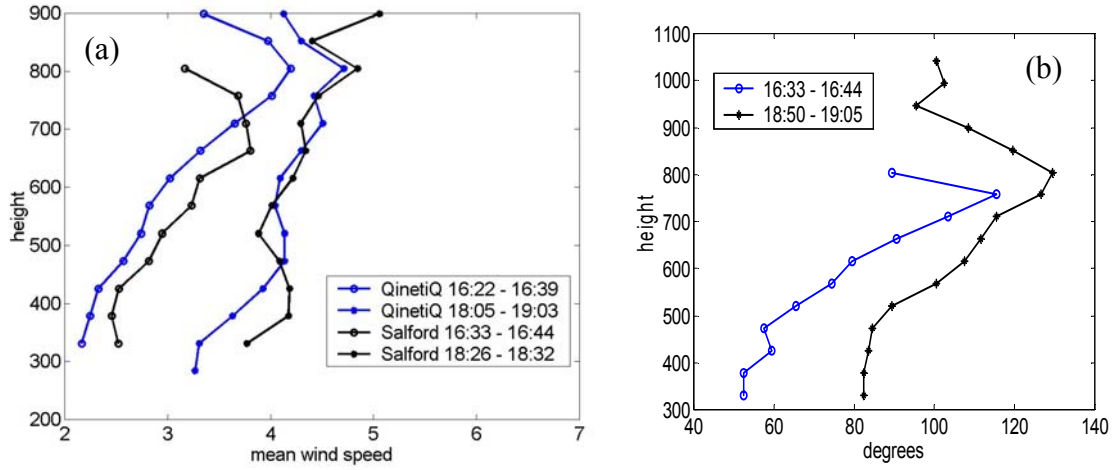

Figure 6.2 (a) Wind speed from VADs with QinetiQ and Salford lidars at approximately 16:30 and 19:00, and (b) wind direction from VADs from Salford lidar at approximately 16:30 and 19:00.

Wind profiles in figure 6.2 show that the mean wind speed is approximately 2.25 ms^{-1} at 300 m above the surface and increases with height. The wind direction is north-easterly at the ground turning to south-easterly at 750 m above the surface.

Following the VAD scans data was taken with the two lidar beams stationary. These fixed beam stares serial 05 were organised so the beams crossed at height of 730 m above the surface as detailed in table 3.3 of report ISB52-05.

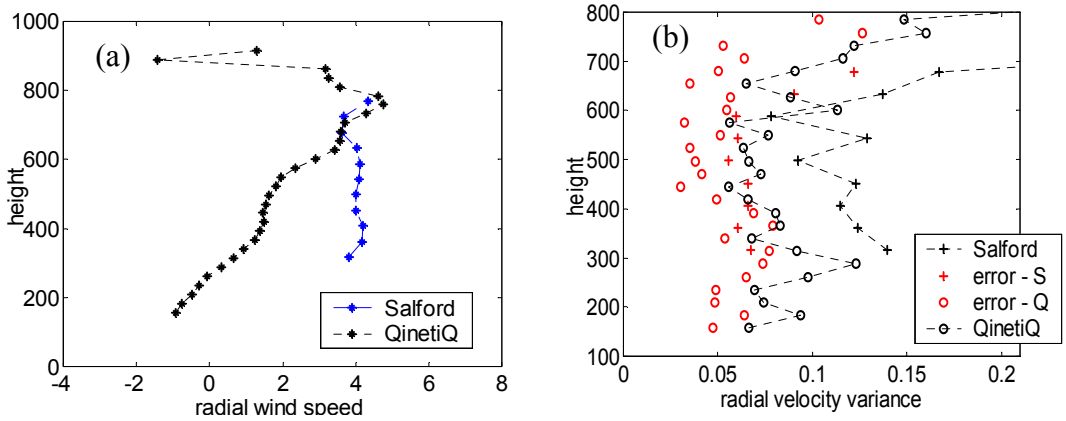

Figure 6.3 (a) The mean wind velocity as measured along the line of sight of the two lidar systems at approximately 18:30 and (b) the wind velocity varaince as measure by the two systems. The red points denote the system estimation error for the two lidars calculated by the method described in Davies *et al* 2003.

The lidar data from the two stare angles are shown in figure 6.3 as line-of-sight velocities and velocity variances. The velocities change with height as a function of both the mean wind speed and mean wind direction. The variances are very small which is typical of evening conditions with light winds where there is little turbulence from either convection or wind shear. Figure 6.3 (b) also shows the estimation error of the two lidar systems which has been calculated using a method detailed in Davies *et al* 2003. The estimation error variance in this case is of the same order of magnitude as the turbulence itself due to the very low turbulence conditions.

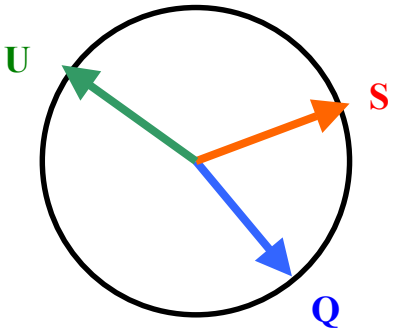

Figure 6.4 Hodograph of the wind direction, U, the angle of the salford lidar beam, S, and the angle of the QinetiQ lidar beam, Q at 730 m above the

Figure 6.4 shows the wind direction at the height at which the two lidar beams cross. It also shows the direction the two lidar beams. From these vectors we can calculate the u and v wind components for mean wind and velocity variance. These two components describe the mean wind velocity and across wind velocity components. The data shown in figure 6.5 is the time-series of data from the point at which the lidar beams cross. The QinetiQ lidar data has been used to calculate the u component of wind and the Salford lidar data has been used to calculate the v component of data. The mean wind velocity variance, u'^2, is 0.15 $m^2 s^{-2}$ from the QinetiQ data and the across wind velocity variance, v'^2, is 0.03 $m^2 s^{-2}$ from the Salford data.

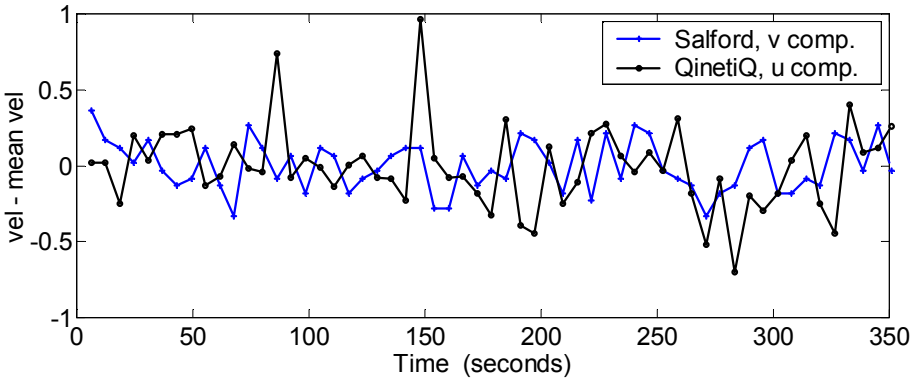

Figure 6.5 The simultaneous data from the two lidar systems plotted as a time-series. Starting time is 18:27:07 UTC.

From the fixed lidar single beam variance data various parameters can be derived. Figure 6.6 shows the covariance spectrum as calculated from the lidar data using the method described in Gal-Chen *et al* 1992 for data on the 13th March at 15:48.

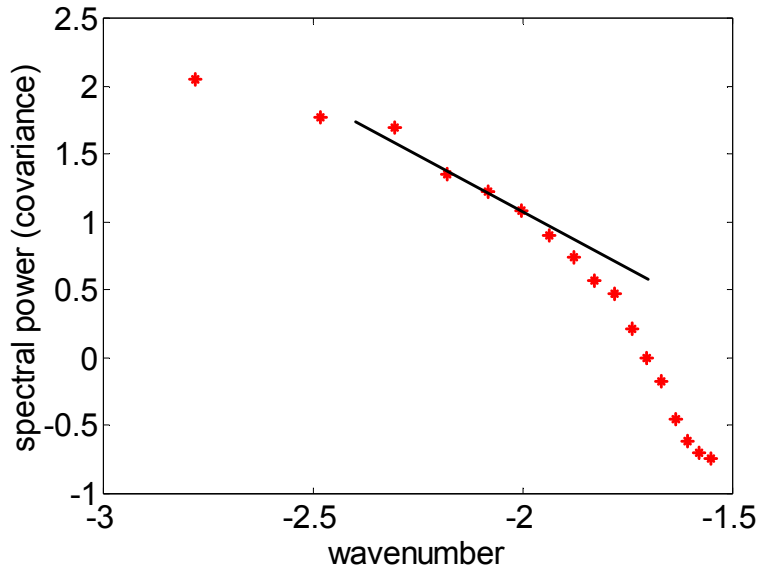

Figure 6.8 Covariance spectrum for Salford lidar data on 13th March at 15:48 UTC. The black line shows the fitted -5/3 slope.

The -5/3 slope shows the part of the spectrum that defines the *inertial subrange* and therefore the associated kinetic energy dissipation rate. For this example the kinetic energy dissipation rate ε is 1.2 x 10^{-3} m^2 $s^{-3.}$ This data from March 13th 2003 was used since the data was measured earlier in the day and shows the higher levels of turbulence consistent with convection i.e. clear sunny weather. Values from other days were 10^{-4} to 10^{-3}. It is a useful result for the NAME model that the Lidars are able to provide data from which ε can be estimated. Eventually, profiles of ε versus height z may be obtained from this work.

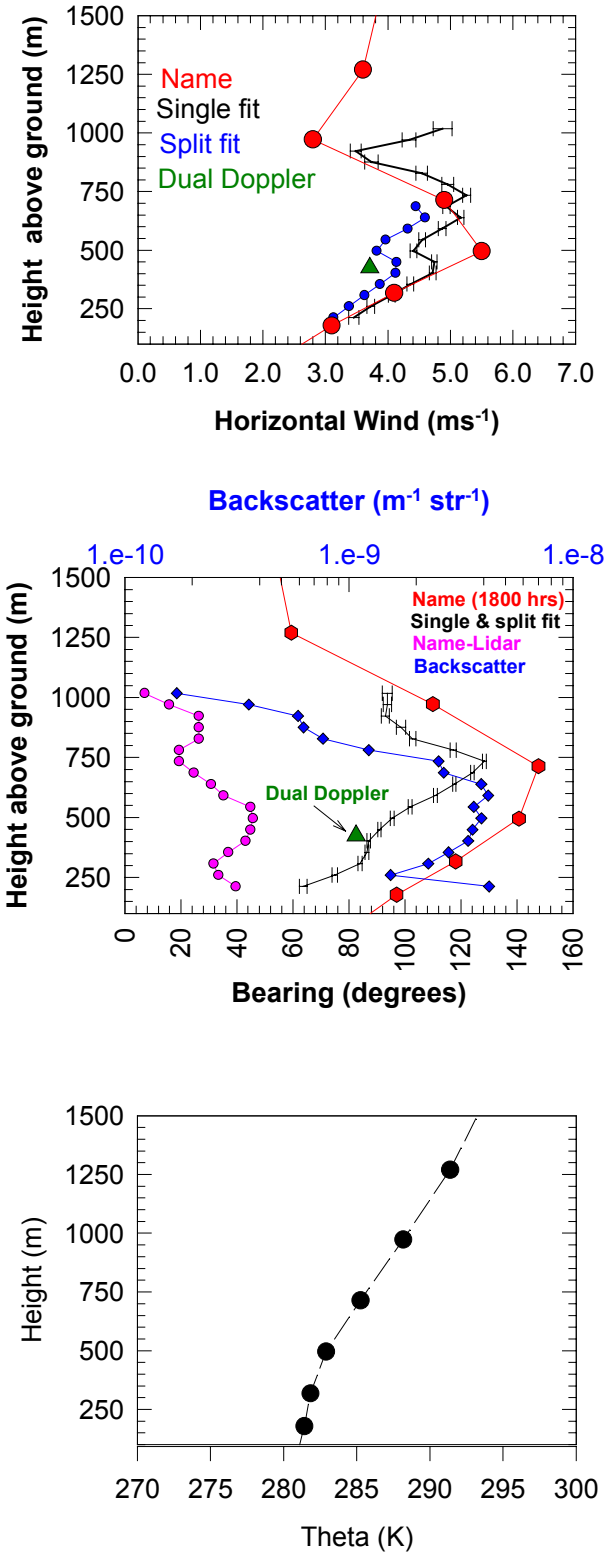

Figure 6.9 Top panel: The wind speed versus height as derived using two different VAD analyses (blue, black), dual Doppler (green) and the NAME model (red). Middle panel: The direction of the wind (VAD (black), dual Doppler (green) and NAME (red)) and the backscatter coefficient (blue) versus height. Bottom panel: The NAME potential temperature versus height.

The upper two graphs of figure 6.9 were shown in an ISB-52 technical working paper Pearson (2003). They are shown again here in conjunction with the potential temperature graph below in order to enable the issue of defining the boundary layer depth to be discussed. The parameter of interest here is the height in the lower

atmosphere up to which any sources at or near the surface will be mixed. This may correlate with various features of the lidar data but the aim is to find the most robust technique for assessing this height both in the daytime and at night. Since any sources will be confined to this layer it is important to try to obtain the most representative height.

The lidar data from which the bearing, wind speed and backscatter values were derived was acquired between 18:50 and 19:03 of the 18th March 03. The potential temperature graph shows data from the NAME model for 18:00 of the same day. The lidar data shows a reduction in the backscatter at approximately the same height as the wind field exhibits a change of direction and a change in speed. This height is about 750m. The potential temperature plot shows a change in gradient at a height of about 450m.

In addition to the wind direction/speed and backscatter the lidar can also yield relative levels of velocity turbulence versus height. Two further data sets have been analysed in order to examine how this turbulence may correlate to the other lidar measured quantities.

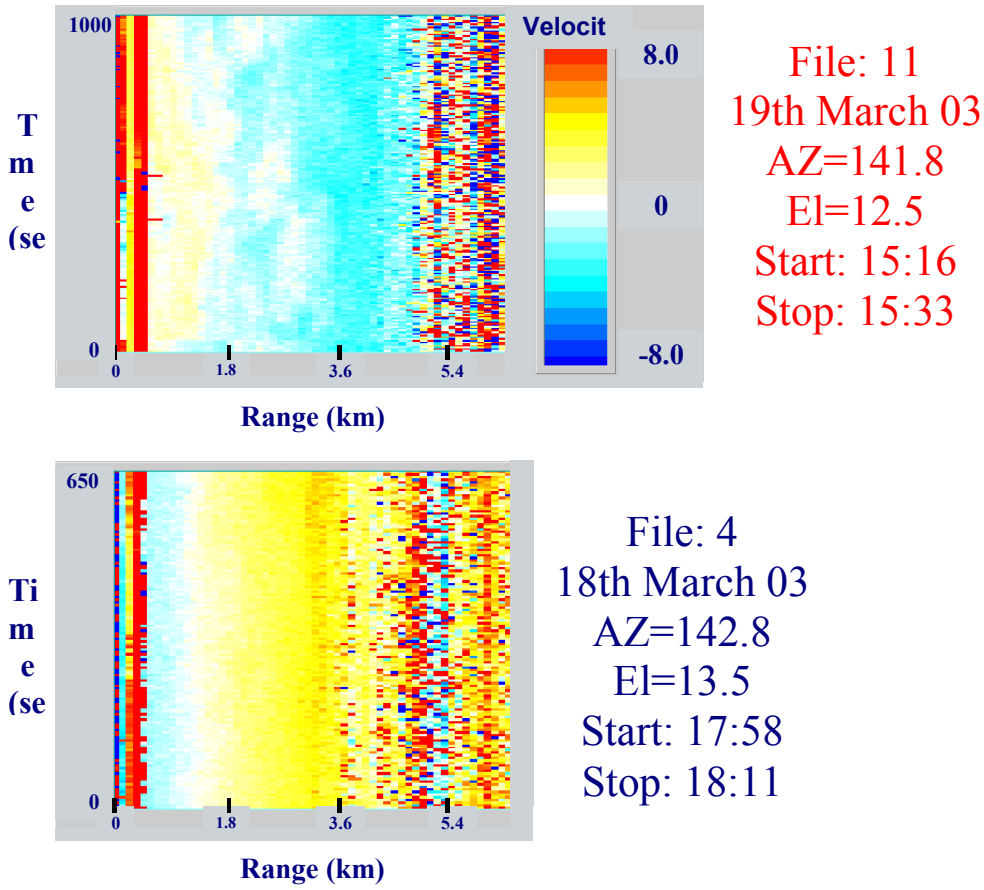

Figure 6.10 The range/time/velocity plots of files 4 & 11.

The two data sets illustrated in figure 6.10were taken on consecutive days in March. It can be seen from the colour plots above that the File 11 data shows more

variability in the wind field than the File 4 data. The time series of velocity estimates for various range gates have been further examined in order to quantify the levels of velocity turbulence.

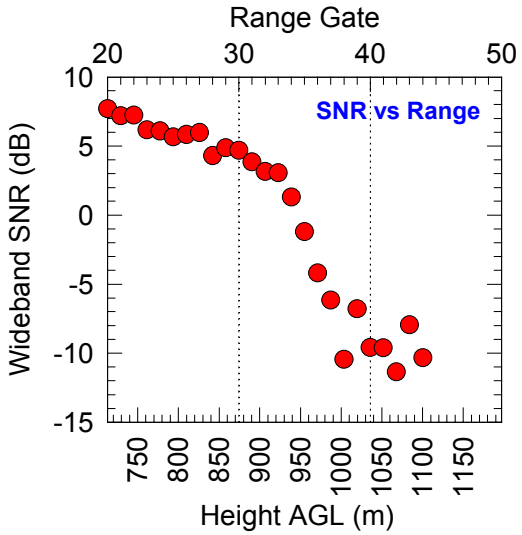

Figure 6.11 The SNR versus range for the first integration set of file 11

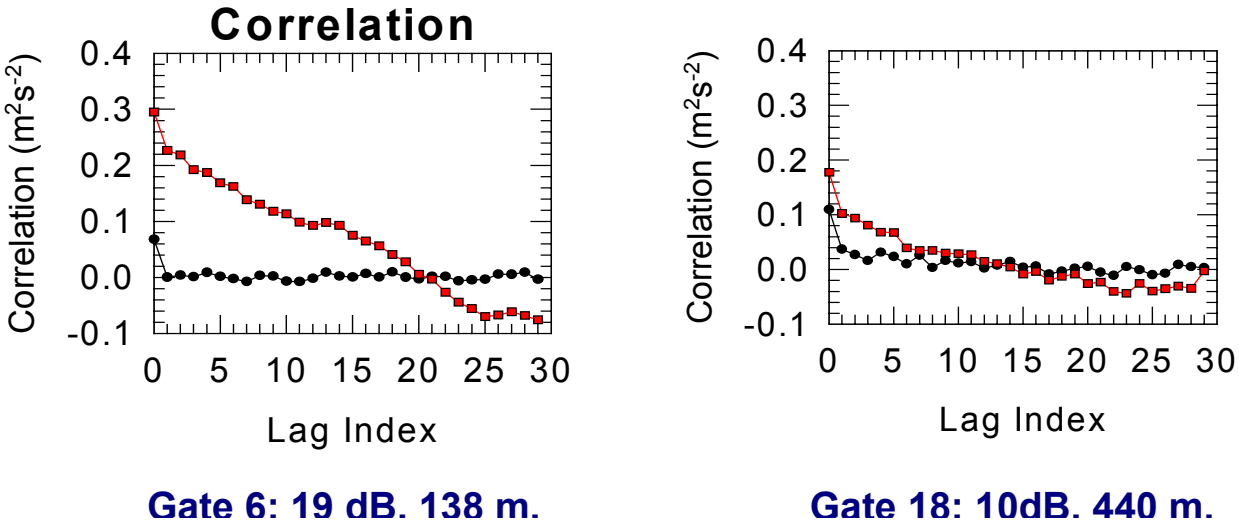

Figure 6.12 The autocorrelation of the velocity estimates for file 4 and file 11 for range gates 6 and 18.

Figure 6.11 shows the lidar SNR versus range gate/height. Above range gate 30 the gradient of the SNR increases as the level of backscatter starts to fall more rapidly.

Figure 6.12 shows the autocorrelation of the velocity time series for gates 6 and 18. It can be seen that there is more correlation for the file 11 data and the degree of correlation is decreasing with altitude. Figure 6.12 shows the spectrum of the gate 6 time series.

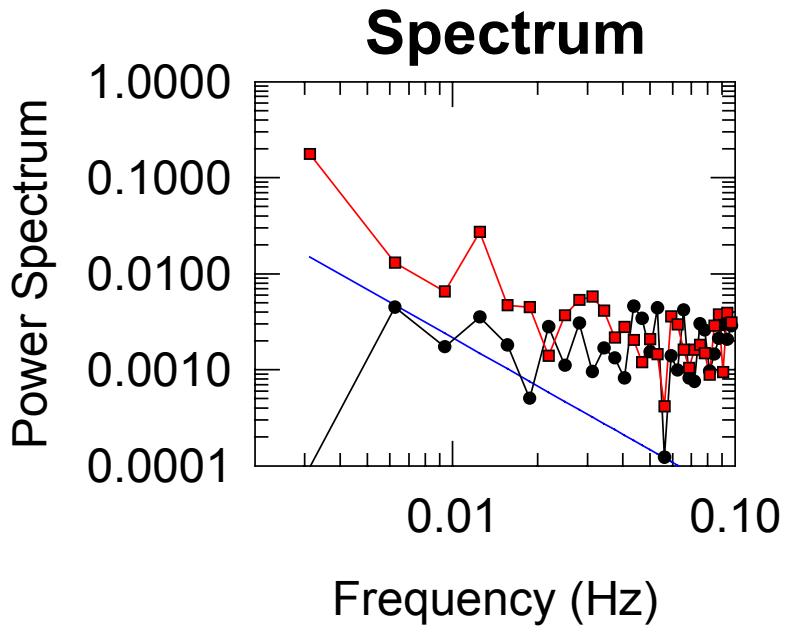

Figure 6.13 The spectrum of the velocity fluctuations for gate 6 of files 4 & 11. The blue line is a -5/3 gradient.

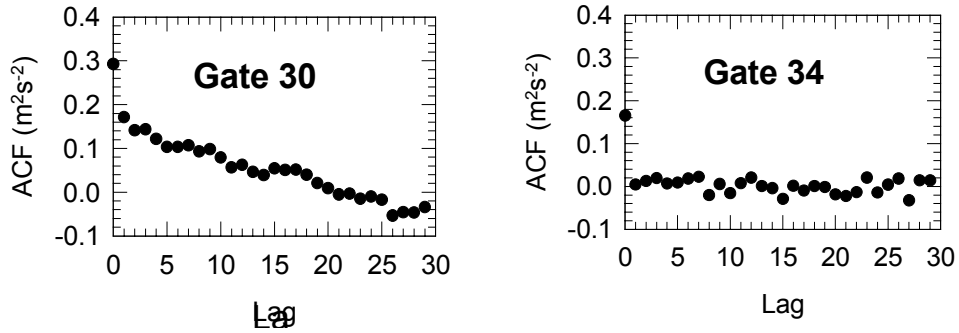

Figure 6.14 The autocorrelation of the velocity time series from file 11 for gates 30 and 34.

Figure 6.13 shows that the top of the more highly scattering layer in the atmosphere was about at gate 30 (875m) at 1530 on the 19th March. Figure 6.14 shows that between gates 30 and 34 the velocity turbulence appears to dissipate. Therefore, for this set of data, there appears to be a reasonably good correlation between the height in the atmosphere that the backscatter starts to fall rapidly and the height at which the velocity turbulence decays.

7. BOUNDARY LAYER DEPTH

The atmospheric boundary layer is a layer near the surface, exchanging heat, momentum and moisture between the earth and atmosphere. Pollutants are dispersed in the this layer. Boundary layer depth or height (of the top of this layer) depends on the wind speed, the vertical gradient of temperature, and the presence of either strong convection or surface cooling. It varies from below 100 m to a few km. It is often greatest in late afternoon, say 1 km, and falls in rural areas to about 100 m in the evening as the ground cools. At night in urban areas, it has a larger value than the rural case. It follows a diurnal cycle.

Since pollutants can be dispersed vertically, we also speak of the mixing layer. The mixing depth represents the height reached by pollutants after release from sources at ground-level. Upward dispersion is eventually limited by an inversion above the mixing layer. Most dispersion models require an estimate of the mixing depth or boundary layer depth/height so that any effective limit on vertical spread can be modelled. The effect is most important when the depth is shallow, when low lying plumes may be trapped near to the ground, or elevated plumes might be unable to reach the ground. The depth may be input to the model, or calculated by routines within the model.

Since the boundary layer depth or inversion height effectively set an upper limit to the vertical mixing of pollutants, they are of great practical importance for dispersion models. In earlier ISB52 reports (report ISB52-01,03 & 04), the boundary layer depth was identified as the highest priority parameter to be determined during the lidar field trials, followed by the wind profile, urban-rural differences, and values of the various boundary layer parameters.

Other workers have measured boundary layer depths by several means, such as the height where turbulence diminishes, or heat flux diminishes, or there is a marked discontinuity in profiles of wind/temperature/moisture, or the height of strong back-returns in acoustic sounding, or from lidar using the aerosol back-scatter signal. However the top of the boundary layer is not easily subject to a unique definition; different methods may yield different values. In this study we are fortunate that the pulsed Doppler lidar can be used to monitor simultaneously both the turbulent fluctuations with height, and the aerosol back-scatter intensity. We may thus compare the decay in turbulent motions with the decay in (from aerosol scatterers) signal intensity (from SNR). As shown below, we find the decay in signal to noise ratio (SNR) which is strongly dependent upon availability of aerosol acting as scatterers, can be employed to detect the top of the boundary layer. This is because we assume the aerosol is largely concentrated in the boundary layer, and there is much less back scatter above the layer. The difference in SNR of the two instruments was $\approx 6dB$, sufficient for the Malvern (QinetiQ) instrument to obtain signal from above the boundary layer top, whilst the Salford one did not. If the SNR of the Salford lidar is improved, then in later trials it may 'see' further. In this trial, the Malvern (QinetiQ) lidar showed a greater decay in SNR at the boundary layer top than either below or past this point. The Salford lidar also has the decay at the top, but saw little beyond it. We suggest from the following results (Section 7.1; Figure 7.1, below) that by plotting the gradient $d(SNR)/dz$ versus z, the point of steepest decay may be located quite distinctly. This hypothesis may form the basis of an objective measure for boundary layer depth (height of BL top), possibly in preference to simply drawing tangents to seek their crossing height. Further work is needed to test this possibility using larger data-sets. The advantage here with these Doppler lidars is that both

criteria, the turbulence and the signal strength may be evaluated for determining BL depth. This is a potentially useful outcome of the first trials.

7.1 Boundary Layer Depth in NAME model.

Numerical Weather Prediction (NWP) data (fields-files) are input to NAME from the Met Office Unified Model; these files include wind speed u, potential temperature θ, etc. at many vertical levels z at every grid-point. The correct magnitude of boundary layer depth is crucial for modelling the advection, dispersion and deposition to the ground, as reported by Maryon et al. (1999). They explained that at the time NAME was first developed, the sensitivity of the modelling to boundary layer depth was somewhat unexpected. It remains a reason for the importance assigned to establishing boundary layer depth in this urban lidar project.

NAME can use the NWP boundary layer depth as calculated by the weather forecast model. this has a numerical value defined at each grid-point. Alternatively, NAME uses NWP data to derive boundary layer depth in two ways (Maryon and Best, 1992; TDN 204):

1. A gradient Richardson Number is calculated for each model layer: the height of the boundary layer is set equal to the height z of the bottom of the layer in which it exceeds a critical value of 1.3 (this value is based upon experience using operational NWP data). The concept being invoked here is well known: boundary layer turbulence is suppressed where the Richardson Number is sufficiently stable (cf. discussion of Richardson Numbers in Sutton, 1953). Thus, stepping up through model layers, evaluate Ri and halt at $Ri > 1.3$, where acceleration due to gravity is g, mean temperature of the layer is $\overline{T}$, and Ri is calculated from the vertical gradient of potential temperature and of wind speed (squared):

$$Ri = \frac{g\,\Delta\theta/\Delta z}{\overline{T}\left(\Delta u/\Delta z\right)^2}$$

2. Parcel ascent method, essentially an adaptation of Holzworth[1] (1974) by Maryon and Best (ibid), to suit the needs of NWP data in the context of NAME. A parcel of air is assumed to have the same temperature as the air near to the ground. For this the NWP model temperature from the first model level was more robust than the surface temperature (which can exhibit large variations). The parcel is allowed to rise, with adiabatic expansion, until neutrally buoyant (equal potential temperatures for the parcel and its surroundings). This defines the boundary layer depth. When NAME calculates the height where the dry adiabat meets the temperature profile, a small temperature offset (0.5-1.5 degrees) is added to the first layer temperature (cf Holzorth[1], 1974, who used 5 degrees). (NB: The dry model was sufficient and computationally quicker to use than virtual potential temperature, which takes water vapour into account.). A dry adiabat Γ_d follows the decrease in temperature with height (9.8 C per km) using Poisson's equation for dry adiabatic expansion, (the pressure decreases as height increases):

[1] The temperature inversion will limit the ascent of thermals from the surface and is a good marker for the depth of the daytime boundary layer. Holzworth (1974) in the USA proposed that ascending air in convective conditions will usually obey a dry adiabat. Consequently the mixing depth can be determined by the height where a dry adiabat from the surface meets the environmental profile of temperature. Holzworth's method has been widely used in the USA. Holzworth had to adjust his method because the radiosonde ascents do not routinely coincide with the minimum or maximum boundary layer depths. Also the ascents are often at sites outside the cities, and some adjustment for urban heating was desired. Holzworth therefore added 5 C to the morning surface temperature.

$$\frac{T_1}{T_2} = \left(\frac{P_1}{P_2}\right)^{R/C_P}$$

and

$$\Gamma_d = \frac{dT}{dz} = -\frac{g}{R}\left(\frac{\gamma - 1}{\gamma}\right)$$

where $R/C_p = 0.286.$ (cf. Sutton, 1953; page 9-10.)

The critical Richardson Number method and parcel ascent method are both calculated in NAME, then the larger of the two boundary layer heights is selected. If the result is small, then it is reset to the minimum value, typically 80 metres:

- The Richardson Number method, which relies upon wind speed and potential temperature profiles, is adopted mostly at night (stable conditions).
- The parcel ascent method, which relies solely upon the potential temperature profile, is mostly adopted in daytime (unstable conditions).

However the exact selection depends upon the temperature and wind speed profiles that are received from the NWP model. Neither method is "aware" of whether it is day or night.

7.2 Boundary Layer Depth in ADMS model

The ADMS met pre-processor can accept a range of options, from which hourly values of the boundary layer parameters are calculated, if not already supplied amongst the input data. These parameters include sensible heat flux Q_H, friction velocity u_*, Monin Obukhov Length L, convective velocity scale w_*, and boundary layer depth h. The met pre-processor is documented in Thomson (2000).

In stable conditions, the heat flux $Q_H \leq 0.0$, and the method of Nieuwstadt (1981) is employed:

$$h = L\frac{0.3u_*}{|f|L}\frac{1.0}{1.0 + 1.9\,h/L}$$

This equation enables h to be calculated hour by hour from L and u_*. The Coriolis parameter $f = 2\Omega\sin\phi$ at latitude ϕ and earth's rotation $\Omega = 7.292\times10^{-5}$ rad sec^{-1}.

In neutral conditions, as L becomes very large,

$$h = \frac{0.3u_*}{|f|}$$

In unstable conditions, the rate of growth of the boundary layer must be solved. Using solar radiation (needed as source of the driving energy) from the sun's position in the sky, cloud cover (needed to modulate the solar input), the sensible heat flux Q_H, friction velocity u_*, Monin Obukhov Length L, convective velocity scale w_*, and boundary layer depth h are calculated. The rate of growth of the daytime boundary layer is modelled on the basis that part of the energy from the sun is input to the convection. The energy reflected varies with the surface albedo (reflectivity). Energy used for evaporation may be described using a modified Priestly Taylor parameter for moisture availability (range 1.0 in desert, 0.5 urban, to 1.0 rural). The growth depends also on the lapse rate of the stable layer aloft. This lapse rate may be input if available. As the turbulence erodes the stable layer aloft, the depth of the boundary layer increases. The model follows Tennekes (1973), Tennekes and Driedonks (1981), Driedonks (1982), with values of constants as in the latter. The value of h at

each hour in the daytime is found by solving the rate of growth of the boundary layer in earlier hours, and varies with time according to conditions.

Near dawn, or sunset, the heat flux is changing rapidly, so additional code is needed to ensure smooth transitions. In ADMS, limits of 50 m and 4000 m are applied to constrain the solution for h.

7.3 Boundary Layer Depth Interpreted from Lidar

Boundary layer depth can be derived from lidar data in various ways. The lidar measures both Doppler wind velocity and backscatter intensity. The backscatter intensity is a function of the system properties, atmospheric attenuation (due to water vapour content of the atmosphere), the returned power (and thus measurement range) and the aerosol loading of the atmosphere. In an urban region, where there is a high atmospheric aerosol concentration, we would expect to get a large backscatter signal for most meteorological conditions. For the trial in Malvern the site was more rural but the weather conditions were conducive to high aerosol concentrations.

At the top of the boundary layer there is a temperature inversion which acts as a lid effectively trapping all the air within the boundary layer. Since most of the aerosols are produced at the surface, above the top of the boundary layer the aerosol concentrations are a few orders of magnitude lower. This change in aerosol concentrations is easily seen in the backscatter intensities measured with the lidar.

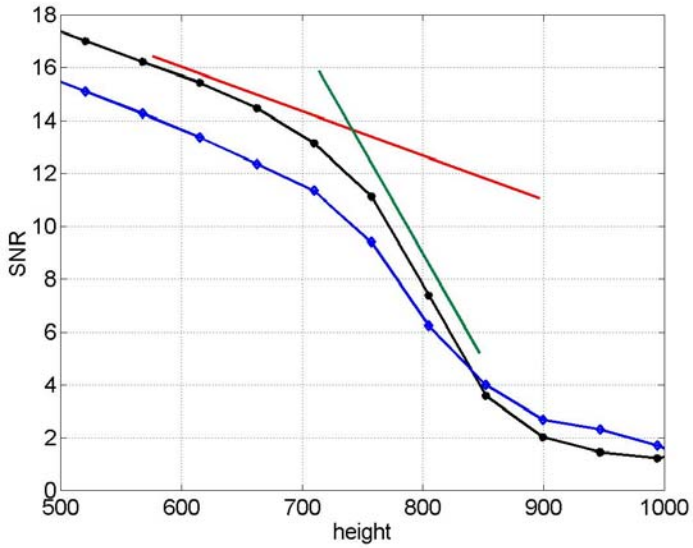

Figure 7.1 Signal to noise profiles from QinetiQ data on 18th March 2003 at 16:00 (black) and at 18:50 (blue). The red and green lines denote the slopes of the SNR due to atmospheric attenuation and the top of the boundary layer respectively.

Figure 7.1 shows the signal to noise ratio (SNR) in decibels calculated from QinetiQ lidar data. The SNR is calculated from the backscatter intensity as follows

$$\mathrm{SNR(dB)} = 10\mathrm{x}\log_{10}\left(\frac{\mathrm{intensity} - \mathrm{noise}}{\mathrm{noise}}\right)$$

The SNR profile in figure 7.1 clearly shows two gradients. The gradient highlighted in red is that due to the normal atmospheric attenuation. The gradient highlighted in

green is a sharper cut off due to the attenuation due to the boundary layer top. The top of the boundary layer can be estimated from the height at which the gradient changes. The blue line in figure 7.1 is the SNR profile on the same day but after sunset . In this case the gradient change is not so well marked. Further analysis must be carried out to investigate this phenomena.

Date	Time (UTC)	Boundary Layer height (m) (QinetiQ lidar)	Time (UTC)	Boundary Layer height (m) (Salford lidar)
13/03/03			16:42	970
17/03/03	16:54	780		
17/03/03	17:13	745		
17/03/03	17:35	755		
17/03/03	18:20	820		
18/03/03	16:02	760		
18/03/03	16:22	690	16:33	675
18/03/03	16:44	690	17:00	700
18/03/03	18:50	760	18:04	730
18/03/03			18:26	710
18/03/03	18:50	760	18:50	710
19/03/03	13:46	835		
19/03/03	14:12	780		
19/03/03	14:24	815		
19/03/03	15:00	840	15:00	860
19/03/03			15:23	845

Table 7.1 Boundary layer height estimated from the SNR of the two lidars

Table 7.1 shows a summary table of the boundary layer heights as measured using the method described above.

7.4 AMDARS Data Processing

The AMDARS work programme (Appendix 1) is summarised by the Met Office team in NWP (Numerical Weather Prediction). Their summary reveals the potential importance of these data to the numerical weather modeling community. For the present study, a computer program was developed to retrieve the AMDARS data from the Met Office archives (MetDB) for the days of the trial, 13-19 March 2003. Latitude and longitude were set to define the region of interest (based on Malvern, but large enough to include Bristol and Birmingham airports). Then the retrieved data were processed to produce plots in a form that could be compared with other data in the Lidar project.

The software retrieves then sorts the data firstly by date and time, then by aircraft identifier. This makes the data easier to follow, such as whether the plane is landing or taking off. The raw data are stored in the MetDB 'as received', in an order which bears little resemblance to events in the real world. Sorting makes it much easier to work with the data. Even so, sometimes data rows have same date, time, latitude and longitude, differing only in altitude. Such niceties are then left to the user to decide if they want then to rearrange any of the data themselves. Planes may be ascending/descending or level flight or on ground; sometimes reported altitude drops to a negative value e.g. -130 m, but the retrieval program currently make no allowances for these details.

The variables in the AMDARS data most relevant to this study are listed below:
At each date/time with a usually but not always unique altitude/latitude/longitude position:
1. Wind speed m/s from plane sensor
2. Wind direction (degrees true) from plane sensor
3. Altitude z (m) from plane altimeter
4. Temperature T (K and C) from plane sensor
5. The QNH correction in the METARS messages to pilots issued by forecasters on the day for the various airfields near/around London was then retrieved in a separate call to another part of the MetDB archives.
6. Pressure P (mbar) derived by the new program code as below.
7. Potential temperature (K and C) calculated as below.

We assumed the altimeters are calibrated to follow the ICAO standard atmosphere. The pressure was derived by converting the altimeter (m) back to an ICAO pressure P(z,ICAO) (mbar). We used Hess (1959) for the equations 6.8, 6.7, and 6.8 respectively in the three lowest layers of this model ICAO atmosphere to calculate P(z,ICAO) from reported altitude z.

We then applied the reverse of the QNH correction (mbar) to estimate the pressure in the atmosphere where the plane happens to be located.

$$P(z) = P(z, ICAO) + (QNH - 1013.25)$$

where 1013.25 mbar is the reference pressure at zero altitude for the ICAO atmosphere. See Roberts (1971) for the ICAO atmosphere, altimetry, and explanatory diagrams. Altimeter setting with explanatory diagrams is defined by Lewis (1991). Also, there is further explanation of altimetry and QNH in the Observers Handbook (1982).

The potential temperature theta (K) was calculated at 1000 mbar standard pressure by Poisson's formula (Hess, 1959; page 31, Equation. 3.16)

$$\theta(z) = T\left(\frac{1000.0}{P(z)}\right)^{R/C_p}$$

where $R/C_p = 0.28541$. When plotting profiles of temperature for use with dispersion studies, this is a useful quantity because it brings all the temperatures at different heights to a common reference pressure, thus removing the temperature change that is normally associated with adiabatic ascent in the atmosphere as the pressure falls. In a thermally neutral atmosphere, there is no change in buoyancy with height, potential temperature is practically constant(as in strong winds on a cloudy day), whilst in stable conditions (on a clear summer night) it increase, or in unstable (sunny days) conditions it decreases with increasing altitude.

Figures 7.2 and 7.3 plot the AMDARS profile of θ versus altitude z for the morning and afternoon of 18 March 2003. They show clearly a mixed region up to 450 m in the morning, or 600 m in the evening. The discontinuity in potential temperature is very clear to see on this day. These Figures were for aircraft at Birmingham airport. There are more AMDARS data available for the London area, simply because the London airports carry so much more air traffic. This will be of value in the next trial when the plan is to run the lidars in West London. The ability to extract measured profiles of temperature over London seems very useful when discussing pollution episodes. In general however there are many more flights by day than night, due to noise restrictions on night flying. AMDARS data are thus most frequent by day.

In evaluating the AMDARS data, some issues arise for further consideration:
1. What further processing of AMDARS might be useful?
2. Did the AMDARS data relate well/badly to other data/observations/model products in the study?
3. Did the profiles generated from the AMDARS seem sensible and were they informative when used with the trials data?

The reader is cautioned that the AMDARS data used in this first field trial are included here for evaluation; we are still exploring its use and validity for use with dispersion studies. There may be further refinements and developments to our AMDARS data processing program in future work. Nevertheless, in the absence of radiosonde ascents at the trials site, the AMDARS data offer potentially useful information on the profiles in the lower atmosphere. In this case, in Figures 7.2 & 7.3 a clear temperature inversion is seen in both the morning at 450-500 m, and late afternoon at 550-600 m of the 18th March 2003.

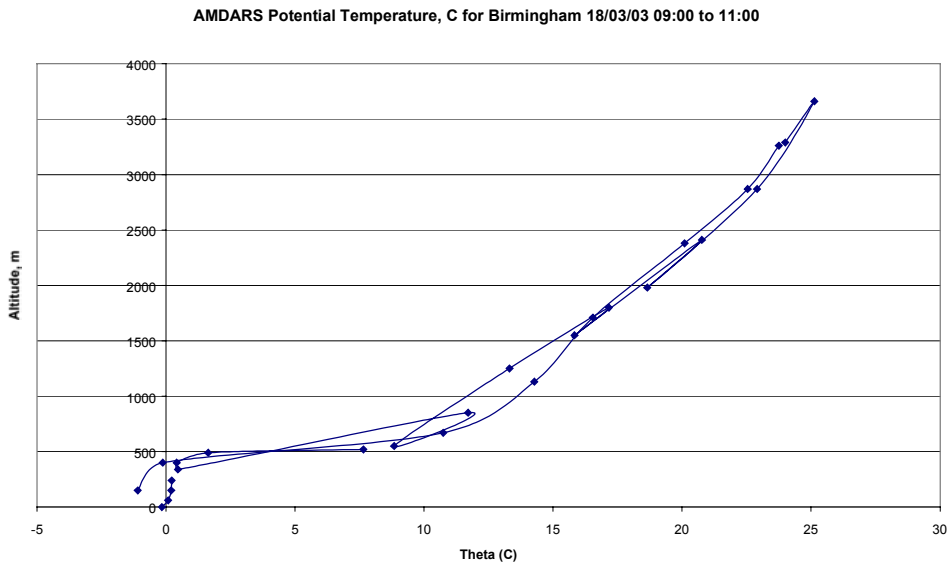

Figure 7.2 AMDARS profile of temperature versus altitude for the morning of 18 March 2003.

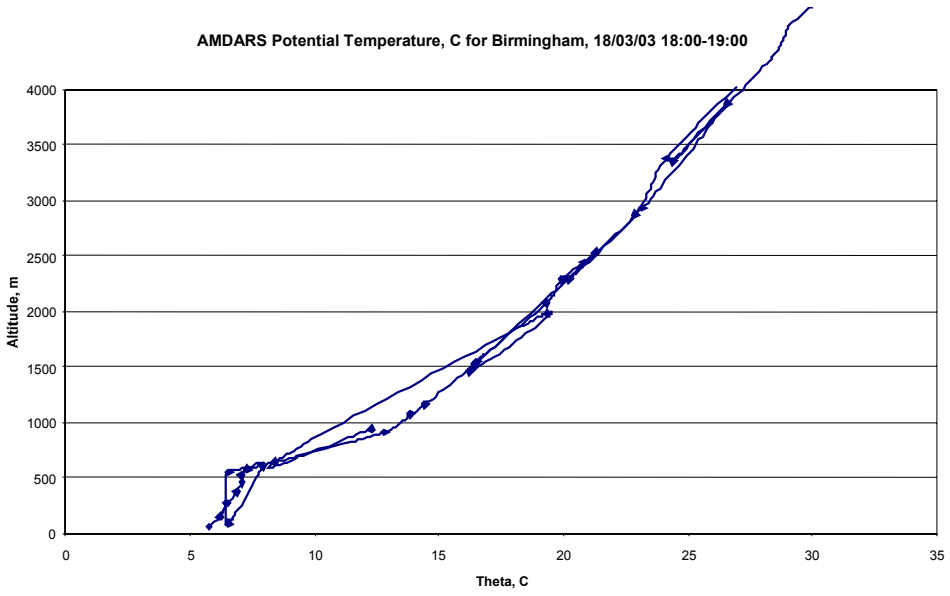

Figure 7.2 AMDARS profile of temperature versus altitude for the afternoon of 18 March 2003.

7.3 Results using ADMS Model

The surface synoptic observations have been retrieved from two Met Office sites: Lyneham and Brize Norton. Both are well exposed, rural airfields. The data were formatted and input into the met pre-processor for the ADMS model. Both stations reported similar observations. The observed cloud cover, Figure 7.4, and wind speed Figure 7.5, were the main input variables.

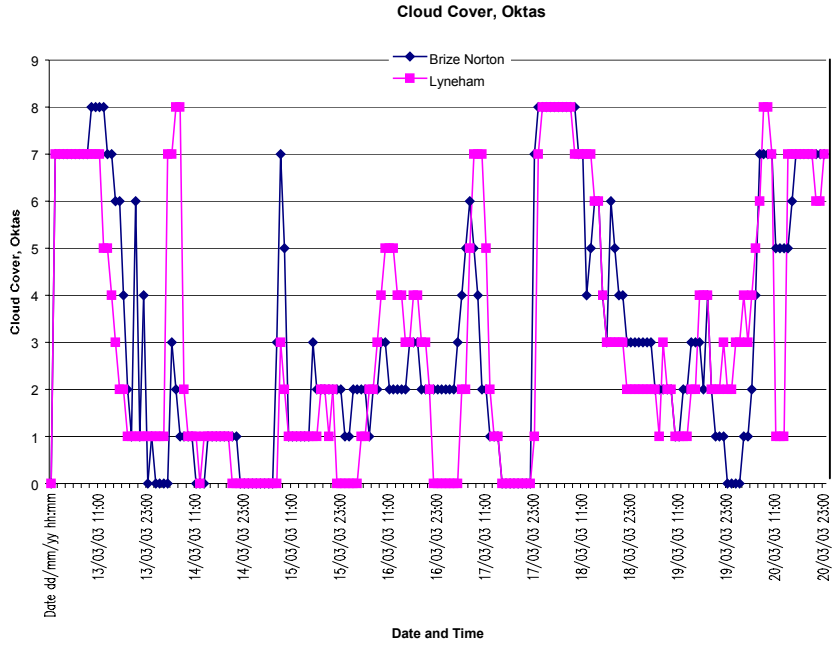

Figure 7.4 Observed values of cloud cover, as input to ADMS met pre-processor.

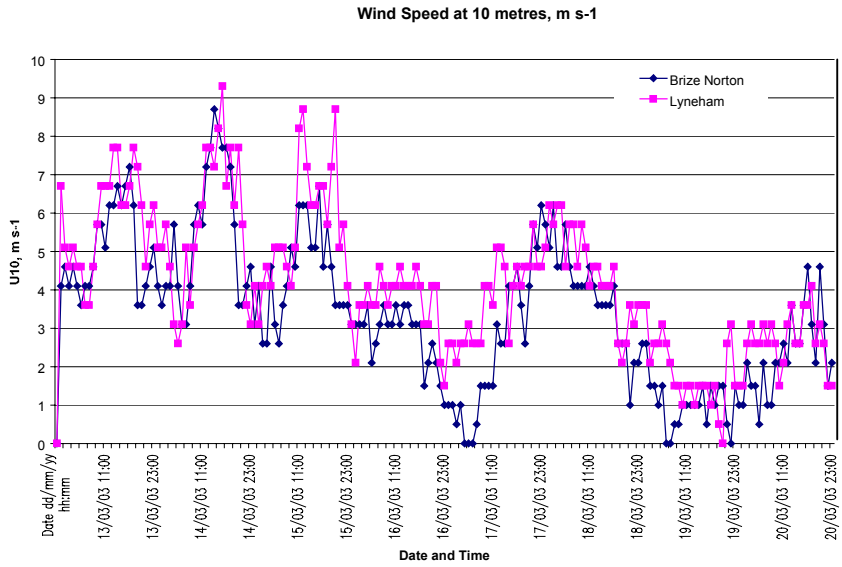

Figure 7.5 Observed wind speed input to ADMS met pre-processor

Results from ADMS now follow. The friction velocity, Figure 7.6, tracks the wind speed (Figure 7.5) fairly well. The sensible heat flux, Figure 7.7, shows the strong diurnal heating and cooling cycle, and so does the boundary layer depth. On this plot

the lidar back-scatter results for BL depth on 13th, 18th and 19th March 2003 appear as pale blue marks. The agreement is quite encouraging, for such sparse data.

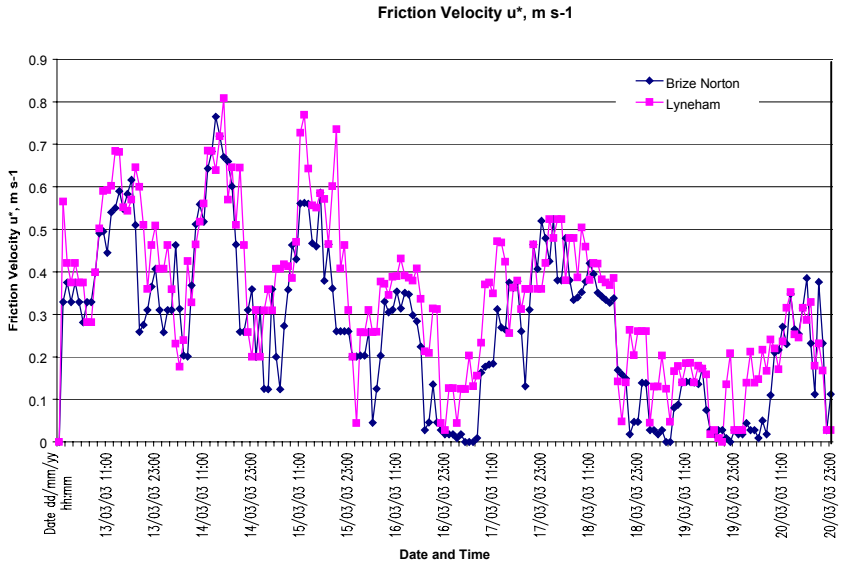

Figure 7.6 Friction velocity calculated by ADMS met pre-processor (an order of magnitude smaller than wind speed above).

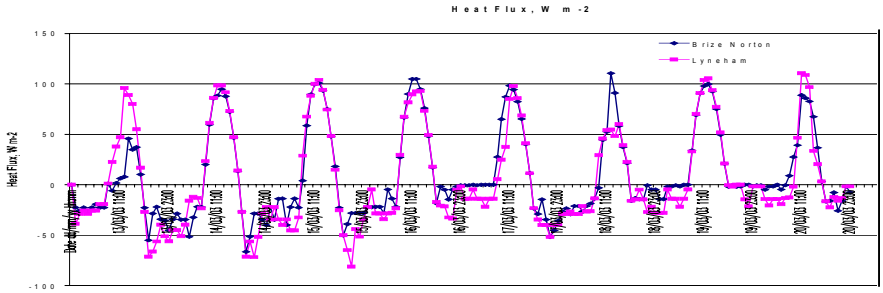

Figure 7.7 The sensible heat flux calculated by the ADMS met pre-processor

Other graphs show the daytime values of the convective velocity scale (it is undefined at night), Figure 7.10, the reciprocal Monin Obukhov length (a dimensional measure of stability, L m,) or $1/L$ m at each station (Lyneham, Figure 7.11, and Brize Norton 7.12, and since $1/L$ is such a difficult variable to plot, we also show its cube root (whilst preserving its sign for stable/unstable) in Figure 7.13.

Several features of ADMS are evident, including the 50 m limit for boundary layer depth in stable conditions (night), and the limiting value of 1.0 for L in stable conditions at a rural site; the latter may be 10 m in the urban ADMS model. The idea of a limit on L is to prevent the equations calculating an unrealistically stable situation. Notice that the cube root plot for $1/L$ is much better at showing the daily changes in stability.

Whilst these Malvern results are encouraging, we await a much fuller data set from an urban environment. This is a goal of the next lidar trial.

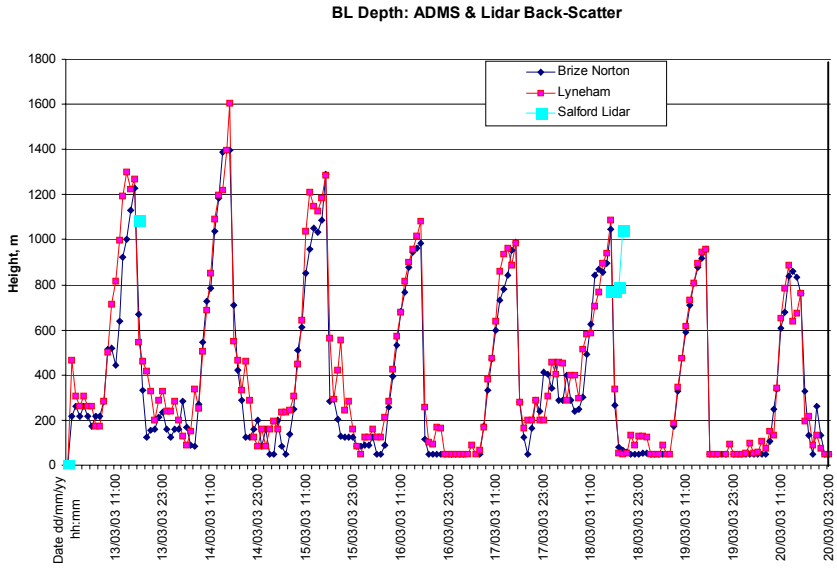

Figure 7.8 Boundary Layer Depths (Heights) calculated by the ADMS met pre-processor; measured data from the Lidar are shown in pale blue.

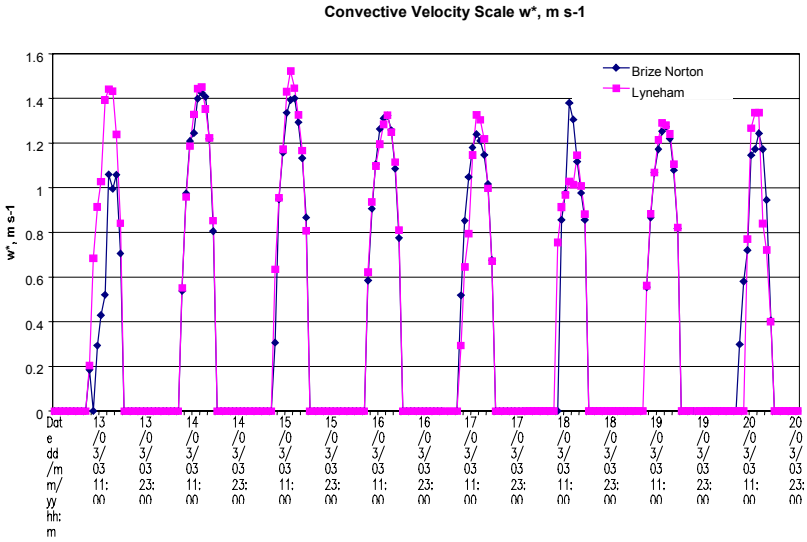

Figure 7.9 Convective velocity scale calculated by the ADMS met pre-processor.

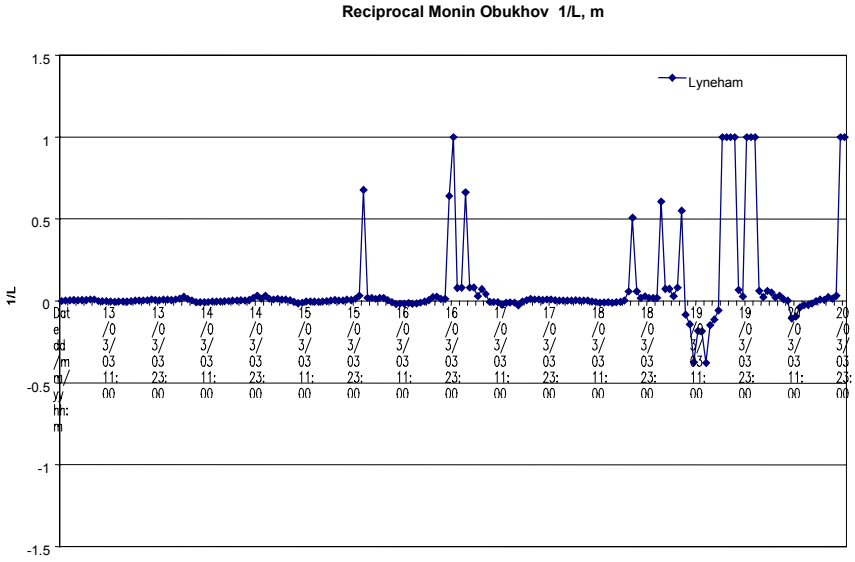

Figure 7.10 Reciprocal of the Monin Obukhov length (stability length scale) calculated at Lyneham by the ADMS met pre-processor.

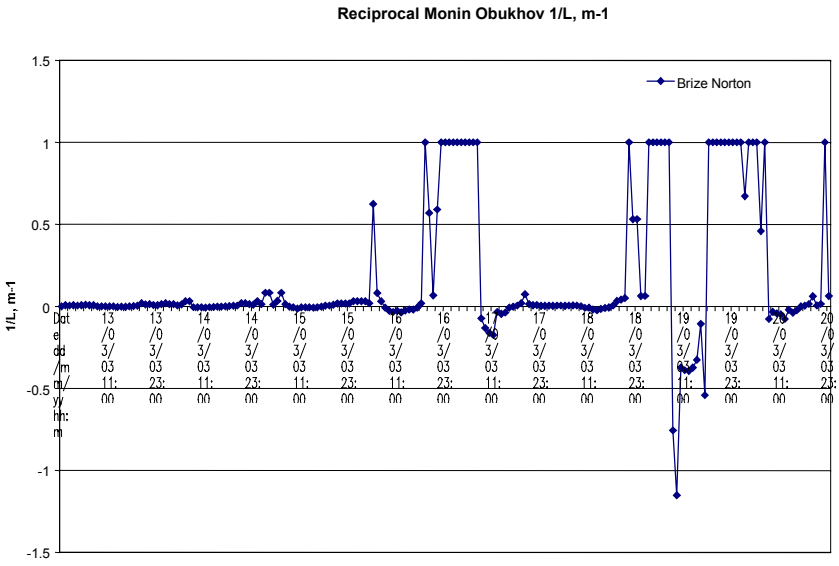

Figure 7.11 Reciprocal of the Monin Obukhov length (stability length scale) calculated at Lyneham by the ADMS met pre-processor.

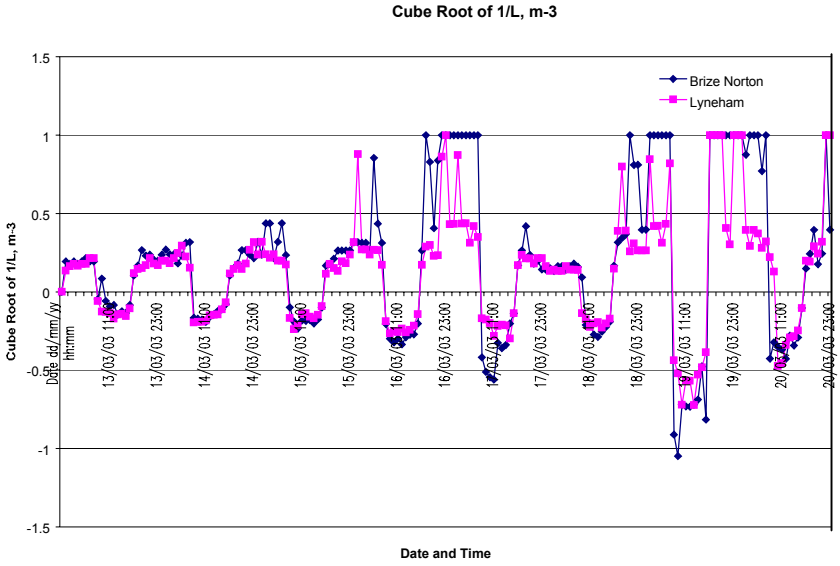

Figure 7.12 The cube root of the reciprocal Monin Obukhov stability length scale, with signs preserved, from values calculated by the ADMS met pre-processor.

8. VISUALISATION OF DATA OF THE MARCH TRIAL

The software to allow the reading and converting of the lidar data has been used for the first time with the dual Doppler lidar data from the March trial. The various data files from both lidars can now, through the two programs *salford2dml* and *qinetiq2dml*, be converted into one single format (DML) data file. These can than be read by DAViS, the visualisation software. Careful usage and small changes to the conversion program may be necessary in the future because the data recording is not a fully automated process.

The visualisation of the March trial data was concentrated around the 3D display of PPI scans and VAD Displays. The visualisation of the PPIs, as shown in figure 8.1, are useful to understand the dimension and location of the data measured by the two lidars. One square of the grid is 1 km^2. A map can later replace the grid and thus gives more information about the area of where the lidars are positioned.

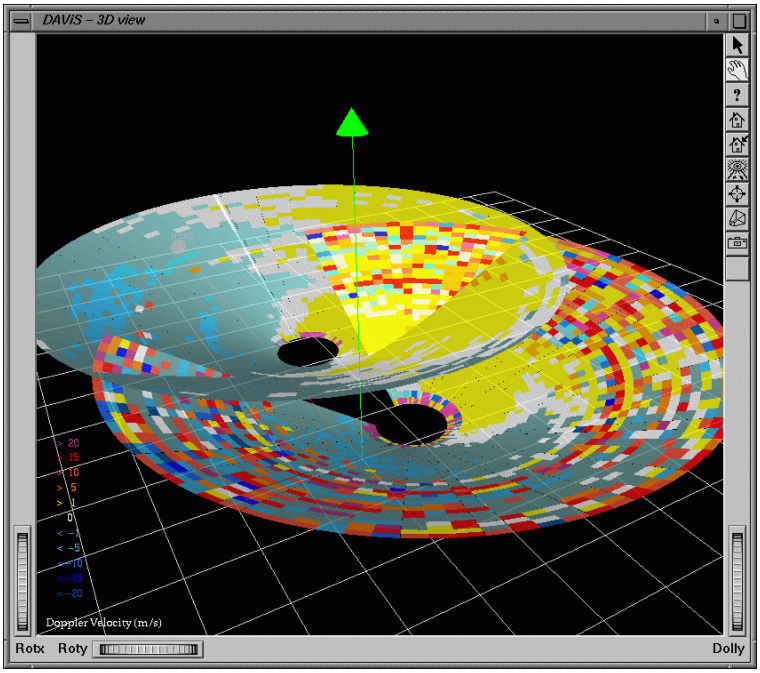

Figure 8.1: Snapshot of two lidar PPIs. The data was measured on the 18th March 2003 at 8:50. The upper left PPI is measured by the QinetiQ lidar, while the bottom right is measured by the Salford lidar.

It is very difficult to portray on paper the full impact of a 3D picture. Such an image is best seen on a screen where it can be animated, since animation (either in time or space) reveals features not apparent in a “snap-shot”. More detail can be seen on the web-site http://prswww.essex.ac.uk/lidar.

A VAD plots the signature of the Doppler velocity depending on the azimuth around the lidar. The DAViS visualisation software allows it to plot VADs from both data sets. Various methods can be used to analyse a VAD signature. DAViS offers the most common methods, such as Least Squares Fits and Fourier analysis as options. Figure 8.2 shows an example of a VAD recorded and the options DAViS gives to analyse the VAD. In Figure 8.2 two forms of the common least squares fit are chosen. It can be seen that the fit, which allows an offset (light green, short dashes), fits better than the fit without an offset (dark green, long dashes). This is an

identification of vertical motion which is uniform over the whole VAD. The offset in Figure 8.2 is about 1 m/s. DAViS will be extended to analyse more accurately the wind field through VADs. A difficulty in analysing a VAD can be seen in azimuths 80 to 110 degrees. The maxima of the VAD signature are often noisy and it is difficult to determine the wind speed. To avoid this problem DAViS will in the future concentrate its analysis on the zero crossings of the signature. However it is desirable that the lidars sample closer than five degrees in azimuth.

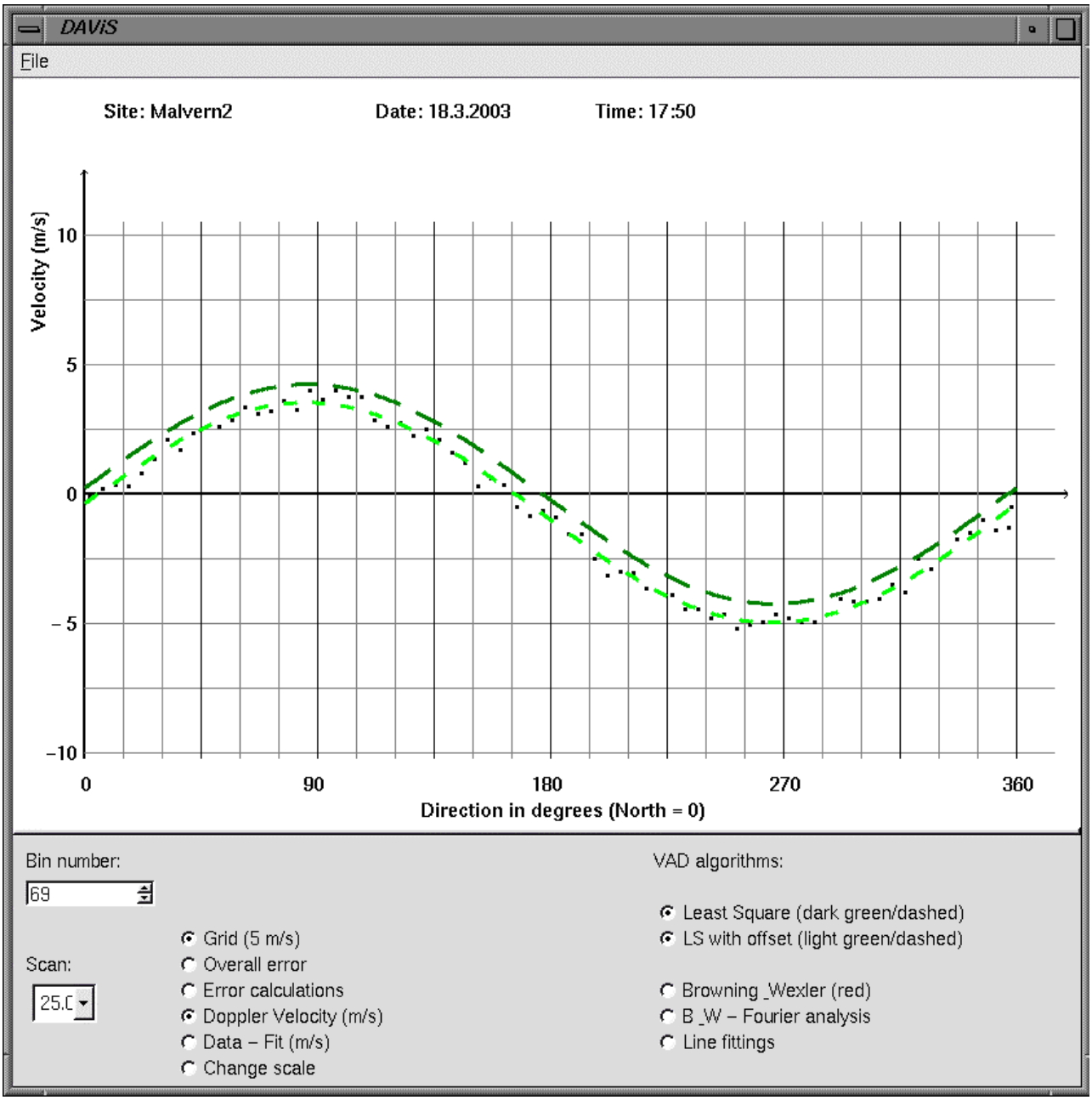

Figure 8.2: DAViS window to analyse VADs. The data shown was measured by the QinetiQ lidar on the 18th March 2003.

9. SUMMARY

The winter Dual Doppler Lidar trial at Malvern has enabled the team to:

1. Deploy Dual Doppler Lidars simultaneously in the field.
2. Develop the technique for alignment of the two beams and locate the intersection point: the team believe this is the first time this has been attempted.
3. Compare the first results for the boundary layer depth obtained in several ways, especially NAME data, ADMS results, Doppler Lidar turbulence profile (as turbulence versus height), aerosol signal decay (as SNR versus height).
4. Evaluate the met pre-processor in the ADMS model using synoptic data as input from available meteorological observing stations.
5. Develop software to retrieve and process AMDARS data: evaluate these results for the potential temperature profile as a separate source of information on the boundary layer, to complement the other observations and model results.
6. Display dual Doppler lidar data as combined results in a sophisticated manner.

The boundary layer depth was identified by the Atmospheric Dispersion Group as a priority, followed closely by the wind and turbulence profiles, and eddy dissipation rate ε,. The latter was estimated as ε~1.2 10^{-3} m^2 s^{-3}, or smaller on some occasions.

The Dual Doppler Lidars have been tested and shown to deliver useful results on these profiles especially at heights that conventional masts cannot reach (these are limited to 45 m in our experience). The improved power and signal to noise ratios of these new instruments means that the turbulence and aerosol concentration can be monitored through the top of the boundary layer.

The first trial results were analysed using tangents to the plot of SNR versus height. This has lead to a new hypothesis that the boundary layer depth may be identified as the height where $\left|\frac{d(SNR)}{dz}\right|$ is greatest, and that this is consistent with the greatest decay in turbulence as well. If the two methods are indeed found consistent, this will give much needed confidence in these data for dispersion modelling. The hypothesis can be tested with the next data sets.

In addition to scientific findings, discussed in the body of the report, a very important conclusion drawn was that it is now appropriate to deploy the equipment at RAF Northolt to measure the flow across rural urban interface, since much experience had been gained and the first results look reasonable. The trial also shows there is a real need for much more extensive deployments of the equipment in the field, to get longer runs of measurements.

As the Project continues, and more trials are conducted in the field, a better data-set of the flow fields, turbulence, and aerosol (fine particles) will emerge. This will enable better visualisation of the models, the field data, and how to improve the air quality forecasting.

10 REFERENCES

Davies F, Collier C G, Pearson G N and Bozier K E (2003) Doppler Lidar Measurements of turbulent structure function over an urban area, *Submitted to J. Oceanic and Atmos. Technol.*

Drobinski P, Dabas A M and Flamant P H (2000) Remote measurement of turbulent Wind Spectra by Heterodyne Doppler Lidar Technique. *J. Applied Meteorol*., 39, 2434 - 2451.

Gal-Chen T, Xu M and Eberhard W L (1992) Estimations of Atmospheric Boundary Layer Fluxes and Other Turbulence parameters from Doppler Lidar Data*. J.Geophys. Res*.**, 97** 18,409-18,423

Hess S L (1959) Introduction to Theoretical Meteorology, Chapter 6, especially Sections 6.3-6.4, and Equations 6.7, 6.8.

Holzworth G C (1974) Climatological aspects of the composition and pollution of the atmosphere. World Meteorological Organisation No. 393 Technical Report No. 139 pages 18-23.

Lewis R N (1991) Meteorological Glossary 6th Edn., Met Office, HMSO, London.

Maryon R H and Best M J (1992). NAME, ATMES and the Boundary Layer Problem. Met Office Turbulence and Diffusion Note No. 204. Met Office London Rd Bracknell Berks RG12 2SZ, UK.

Maryon R H, Ryall D B and Malcolm A L (1999). The NAME 4 Dispersion Model:Science Documentation. Met Office Turbulence and Diffusion Note No. 262. Met Office London Rd Bracknell Berks RG12 2SZ, UK.

Mayor S D, Cohn S A, Lenschow D H, Grund C J and Hardesty R M. (1997) Convective Boundary Layer Vertical Velocity Statistics Observed by 2 μm Doppler Lidar. *Proceedings of the 9th Conference on Coherent Laser Radar, June 23-27, Sweden. 256-259*

Observers Handbook (1982) The Observers Handbook. 4th Edn., Met Office, HMSO, London. Chapter 7, Sections 7.4-7.6, and 105-106. Page 98 defines pressure units in meteorology.

Pearson G N and Collier C G (1999) A pulsed coherent CO2 lidar for boundary layer meteorology. *Q. J. R. Meteorol. Soc*., **125,** 2703 - 2721.

Pearson GN and Willetts DV (2003). Assessment of lidar performance ad data from the first dual Doppler lidar trial. TWP ISB-52 March 2003.

Roberts E D (1971) Handbook of Aviation Meteorology, 2nd Edn. Sections 8-9, pp. 13-19. the Met Office, HMSO.

Rye B J and Hardesty R M (1993) Discrete spectral peak estimation in incoherent backscatter heterodyne lidar. II Correlogram accumulation*. IEEE Trans. Geosci. Remote Sens*., **31**, 28 - 35.

Sutton O G (1953) Micrometeorology. A Study of Physical Processes in the Lowest Layers of the Earth's Atmosphere. McGraw Hill, London.

Thomson D J (2000) The Met Input Module. ADMS Model Document P05/01J/00. Available from CERC Ltd, Cambridge, UK, or Atmospheric Dispersion Group, Met Office, Bracknell, Berkshire RG12 2SZ.

11 GLOSSARY

ADMS	-	Atmospheric Dispersion Modelling System dispersion model from CERC
AEOLIUS	-	A dispersion model used by the Met office
AERMOD	-	A dispersion model from the American EPA.
BOXURB airflow	-	A dispersion model developed by the Met Office to describe through an urban canyon modelled as a box.
CW	-	Continuous wave
EPA	-	Environmental Protection Agency, a US government organisation
FWHH	-	Full width half height, a measure of the depth of field of the sensing zone of a CW lidar.
ISB	-	Invest to Save Budget
ISC	-	Dispersion model
LATAS	-	Laser Airborne True Airspeed sensor, an early Malvern Lidar
LDV	-	Laser Doppler Velocimeter
LDV1	-	Laser Doppler Velocimeter 1 (A Lidar developed at Malvern).
MRU	-	Met Office research unit
NAME	-	Main dispersion model used by the Met Office
NWP	-	Numerical weather prediction
RAM	-	A dispersion model
RHI	-	Range height indicator
TEA Dioxide	-	Transfer exited atmosphere (pressure). A type of Carbon lasers that emits pulses of relatively high energy. Used in the pulsed lidar to achieve measurements to greater ranges.

APPENDIX 1. The AMDARS Programme

AMDARs (Aircraft Meteorological Data Reporting) systems are carried on-board aircraft and automatically measure various atmospheric parameters the results of which are then sent to data receiving centers for use in numerical weather prediction models.

The Role of AMDAR

AMDAR systems operate on aircraft which are equipped with sophisticated navigation and other sensing systems. There are sensors for measuring air speed, air temperature and air pressure. Other data relating to aircraft position, acceleration, and orientation are available from the aircraft navigation system. The aircraft also carry airborne computers for the flight management and navigation systems, by which navigation and meteorological data are computed continuously and made available to the aircrew at the flight deck. In AMDAR systems this information is further processed and fed automatically to the aircraft communication system for transmission to the ground. Alternatively a dedicated processing package can be used on the aircraft to access raw data from the aircraft systems and independently derive the meteorological variables.

In AMDAR systems these facilities are used to compile and transmit meteorological reports in real time. The messages contain wind speed and direction, air temperature, altitude, a measure of turbulence and the aircraft position.

The source data for meteorological observations require significant correction and complex processing to yield meteorological measurements representative of the free air-stream in the vicinity of the aircraft. Although the data processing involved it quite complex, errors in reported wind and temperatures are comparable with those of radio-sonde systems. Thus AMDAR observations can provide high quality single level data in cruise and detailed profile data up to cruise levels.

Indeed AMDAR observations can meet the resolution and accuracy requirements for global NWP. Observations are restricted from commercial aircraft to specific air routes at cruise level and profile data are only available on climb or descent in the terminal areas. It should also be noted that AMDAR observations are not made at standard times and thus significant gaps in observations arise due to the normal flight scheduling.

AMDAR profiles can be very useful for local airfield forecasting and are available during flight operations. This can be especially important during severe storm events.

AMDAR Communication systems

ASDAR (Aircraft to Satellite Data Relay) data are transmitted from the host aircraft via the International Data Collection System (IDCS) on board the Meteorological Geosynchronous Satellite System (Meteosat, GOES E, GOES W, GMS). Ground stations are located in the USA, Japan and Europe where the received data are encoded into WMO AMDAR code and injected into the GTS (global telecommunications System used for international exchange of meteorological data).

The EUMETNET-AMDAR Project

The EUMETNET-AMDAR Programme has been set up to maximise the cost/benefit ratio of AMDAR systems operated by the participating members by reducing duplication and seeking to meet requirements in the most cost effective manner. The participating members are as follows:

Austria, Denmark, Finland, France, Germany, Iceland, Ireland, Luxembourg, Netherlands, Norway, Portugal, Spain, Sweden, United Kingdom

To date AMDAR programmes have been set up by KNMI (The Dutch Met Service), SMHI (The Swedish Met Service), Météo-France, DWD (The German Met Service) and the Met Office.

A need to co-ordinate European AMDAR efforts has been identified, and as a result the EUMETNET-AMDAR programme has been set up and is being managed by Bruce Truscott. This programme started on January 1st 1999 and represents a short term optional programme with a duration of three years. It is hoped that it will deliver an AMDAR programme to meet the following objectives:

To provide ascent/descent measurements over the territory of EUMETNET members, aiming at an average spacing of 250km and a time spacing of every 3 hours, to be adjusted as necessary according to the results of the EUCOS design studies. To provide measurements from data sparse areas having an impact on short range forecasts in Europe, to be adjusted as necessary according to the results of the EUCOS design studies. Measurements from data sparse areas world-wide, representing about 20% of the data collection effort of the programme.

Over recent years it has become evident that significant valule of meteorological data can be obtained from large areas of the World by collection data from aircraft fitted with appropriate software packages. To date the predominant sources of automated aviation data have been from ASDARs, and more recently ACARS (Aircraft Communication Addressing and Reporting System) equipped aircraft.

ACARS systems, route data back via general purpose information processing and transmitting systems now fitted to many commercial aircraft. Such systems offer the potential for a vast increase in the provision of aircraft observations of wind and temperature.

The various systems (ASDARS,ACARS) are collectively named AMDAR (Aircraft Meteorological Data Reporting) systems and are making an increasingly important contribution to the observational data base of the World Weather Watch (WWW) of the World Meteorological Organisation. It is envisaged that AMDAR data will inevitably supersede manual air reporting (AIREPS).

In recent years the Numerical Weather Prediction (NWP) community's requirement for capturing ever increasing amounts of automatic meteorological data from aircraft has grown, and with this the programme to investigate the means of capturing this data. The result of this requirement has been the setting up of several national MDAR programmes, some of which are operational and some still in the planning stage.

12 ACKNOWLEDGEMENTS

This work was funded by HM Treasury under the Invest to Save Budget. Department for Environment, Food and Rural Affairs (DEFRA) acted on behalf of HM Treasury. QinetiQ work described herein was supported under Contract Number CU016-0000014438 and this support is acknowledged.

The authors also acknowledge assistance from members of the Met Office for the meteorological data herein. In particular D J Thomson who advised on the ADMS Boundary Layer scheme and D B Ryall for the NAME data retrievals.

13 DISCLAIMER

The authors of this report are employed by QinetiQ, the Met Office, Salford University and Essex University. The work reported herein was carried out under a Contract CU016-0000014438 Version 1.0 placed on 26 October 2001 between QinetiQ and the Secretary of State for Environment, Food and Rural Affairs. Any views expressed are not necessarily those of the Secretary of State for Environment, Food and Rural Affairs.

© Copyright 2003

14 DISTRIBUTION LIST

Copy No.	Name	Address
1-4	Dr Janet Dixon	DEFRA
5	Prof D V Willetts	PD315, QinetiQ Malvern
6	Dr G N Pearson	PD313, QinetiQ Malvern
7	Dr R I Young	PD115, QinetiQ Malvern
8-11	Dr D Middleton	Met Office, London
12	Prof C Collier	Salford University
13	Dr F Davies	Salford University
14	Dr K Bozier	Salford University
15	Prof A Holt	Essex University
16	Dr G Upton	Essex University
17	Dr S Siemen	Essex University
18	Project File	PD115, QinetiQ Malvern

Copy No.	Name	Address
19-23	Spares	PD115, QinetiQ Malvern